EurJOC
European Journal of Organic Chemistry

Full Papers
doi.org/10.1002/ejoc.202100044

Chemistry Europe
European Chemical Societies Publishing

Special Collection

Noncovalent Interactions between Stacked Arenes in 1,8-Bis-(1-naphthyl)-naphthalenes

Michel Chiarucci,[a] Andrea Mazzanti,[b] Paolo Righi,[b] Giorgio Bencivenni,[b] and Michele Mancinelli*[b]

Dedicated to Professor Franco Cozzi on the occasion of his 70th birthday

A number of 1,8-bis(1-naphthyl)-naphthalenes, bearing different substituents in the 1-naphthyl moieties have been prepared to investigate the noncovalent interactions between the stacked arenes. The best geometries were determined by means of DFT calculations, and experimentally checked by NMR and electronic circular dichroism (ECD). High temperature NMR spectroscopy allowed for the determination of the balance between dispersive and electrostatic contributions (ratio between two diastereomeric *syn/anti* isomers of compounds **1–6**), while ECD analysis of the *syn* isomers of compounds **3–5** allowed for a deeper insight on the electrostatic contributions that drive the geometry between the interacting rings. The two rings preferentially adopt a parallel displaced geometry, whose interaction energy is strongly influenced by the electrostatic features of the two naphthyl rings, and that dispersive forces play a very minor role.

Introduction

"This finding, together with other experimental evidence leads us to conclude that a significant through-space polar-π exists between the two phenyl units."[1]

Since the Cozzi's intuition in 1992, the studies of non-covalent interactions between aromatic rings have shown that they strongly influence a variety of chemical processes.[2] They have been used in the template-directed synthesis of complex supramolecular adducts,[3] and in the explanation of the stereochemical outcomes of enantioselective reactions.[4] They are decisive for crystal packing and engineering,[5,6] to determine the structures of biomolecules such as nucleic acids and proteins,[7] and to mediate molecular recognition events involving proteins,[8] carbohydrates,[9] and drugs.[10]

While the benzene dimer has been widely used as a paradigmatic prototype for the development of simple models of π-stacking interactions,[11] for many years the two "classical" models for description of stacking interaction were the electrostatic model and the "polar-π" approach proposed by Hunter and Sanders[12] and by Cozzi and Siegel,[1,13] respectively.

However, results presented by Sherrill showed that in the case of the benzene dimer[14] substituents with opposite electronic effect stabilize in any case the sandwich dimer, in contrast with the Hunter-Sanders model. Further studies showed that the benzene dimer had to be considered such as a separate case, while all the stabilizing effects of the substituents should be ascribed to dispersive interactions.[15] In 2011, an upgrade to this theory proposed that the effects of the substituents are effective only in a narrow region of space near to the vertex of the substituent, while the remaining part of aromatic ring is not affected.[16] During the years, some authors also questioned the whole significance of the terminology applied to the noncovalent interactions.[17,18]

In this paper, we present the preparation and the conformational analysis of a series of 1,8-bis-(1-naphthyl)-naphthalenes with various levels of fluorination and substitution at the two rings bonded to the central skeleton (Scheme 1).

The two facing rings, occupying the 1,8 position of the third naphthalene, act mutually to yield attractive or repulsive interactions. The best geometries are calculated using Density

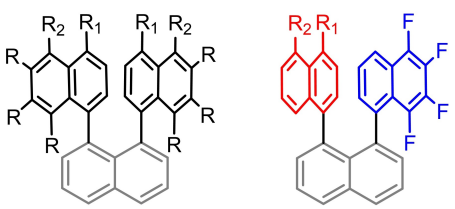

1 R=R$_2$=H, R$_1$=Me
2 R=R$_2$= F, R$_1$=H
6 R=R$_1$=H, R$_2$=OMe
3 R$_1$=Me, R$_2$= H
4 R$_1$=OMe, R$_2$=H
5 R$_1$=H, R$_2$=OMe

Scheme 1. Compounds investigated in this manuscript.

[a] Dr. M. Chiarucci
Polycrystalline S.p.A
Via della Cooperazione 29, 40059 Medicina, Italy
[b] Prof. Dr. A. Mazzanti, Prof. Dr. P. Righi, Prof. Dr. G. Bencivenni, Dr. M. Mancinelli
Department of Industrial Chemistry "Toso Montanari" and INSTM Research Unit Bologna
University of Bologna
Viale Risorgimento 4, 40136 Bologna, Italy
E-mail: michele.mancinelli@unibo.it

Supporting information for this article is available on the WWW under https://doi.org/10.1002/ejoc.202100044

Part of the "Franco Cozzi's 70th Birthday" Special Collection.

© 2021 The Authors. European Journal of Organic Chemistry published by Wiley-VCH GmbH. This is an open access article under the terms of the Creative Commons Attribution License, which permits use, distribution and reproduction in any medium, provided the original work is properly cited.

© 2021 The Authors. European Journal of Organic Chemistry published by Wiley-VCH GmbH

Functional Theory (DFT) calculations, and the importance of the various contributions can be experimentally evaluated by measuring the equilibrium populations of the different conformational stereoisomers, as well as the conformational ratio modifications due to the different dielectric constant of the solvent. Electronic circular dichroism spectra (ECD) coupled with TD-DFT calculations are used to determine the conformational preferences of the two interacting rings.

Results and Discussion

When two naphthyl rings are connected to the 1,8 positions of a third naphthalene, the steric hindrance causes the two rings to be skewed out of the plane of the third ring. The two rings are therefore forced to face each other in a very close distance (< 3.4 Å) because of the 1,8-naphthalene scaffold. Among the various known geometries for noncovalent interaction, only the parallel stacked and face-to-face interactions are allowed in this chemical system. The structural constrain prevent the two-naphthyl ring to adopt any edge-to-face arrangement.

The two 1-naphthyl rings of compounds **1,2,6** (Scheme 1) are identical, and in principle only two conformations should exist: a *syn* and an *anti* conformations where the 5,6,7,8 carbons of the 1-naphthyl rings (hereafter *benzo* moieties) are on the same side, or on the opposite sides of the 1,8-naphthyl ring (Figure 1).[19] However, as in the paradigmatic case of biphenyls and binaphthyls, the two ancillary rings are not exactly perpendicular to the 1,8-naphthalene, and this geometric situation implies that two diastereomeric *anti* conformations can exist (Figure 1, bottom).

They can be named as *anti-in* and *anti-out* depending on the value of the dihedral angles being bigger or smaller than |90°| (the dihedral angles to be considered are the 8a–1-1′-8a′ marked as red lines in Figure 1). Both conformations belong to the C_2 symmetry group, thus entailing the existence of a pair of conformational enantiomers (*M, M* and *P, P*. in Figure 1). These two conformations can be exchanged by a low-energy geared pathway where both rings simultaneously "slide" over each other until they reach a perpendicular transition state (the so-called π-barrier).[20] In the case of the *syn* conformation, the same displacement out of the orthogonality does not create diastereomeric conformations: the enantiomer is generated instead (Figure 1).[21] Due to the tiny energy involved in the π-barrier, the *syn* isomer corresponds to a meso form.

In compounds **3–5** the two ancillary rings are different, and the *syn* conformation is split into two diastereomeric conformations (each one with its enantiomeric counterpart, Figure 2). They can be named as *syn*-out and *syn*-in by referring to the dihedral angle of the 5,6,7,8-tetrafluoro-1-naphthyl ring with respect to the 1,8-naphthyl core being larger or smaller than |90°| (*syn*-out and *syn*-in, respectively).

The different dispositions of the two aryl rings in the *anti* and *syn* conformations can represent a good chemical balance to evaluate the effect of through-space interactions between the two arenes.[22] While in the case of the *anti* isomer the two *benzo* moieties of the 1,8-naphthyl rings are far and a stacking interaction can occur only between the *ipso*-benzene rings (i.e. the rings composed by carbons 1,2,3,4,4a and 8a), in the *syn* isomer the two ancillary rings can be arranged in a parallel-displaced relationship.

The theoretical distance between the two centers of the rings when they were exactly perpendicular to the third naphthalene is about 3.3 Å, and that value becomes slightly smaller when the two rings are arranged in a skewed conformation (see Figures S1 and S2 of ESI). In the sandwich dimer of benzene,[23] this distance corresponds to an interaction energy calculated to be close to zero.

Although the *syn/anti* rotational barrier is very high (see below), small variations of the dihedral angles around a perfect orthogonality of the rings with the naphthalene core allows for geometrical rearrangements of the relative distances and stacking geometries of the two rings, with a very small

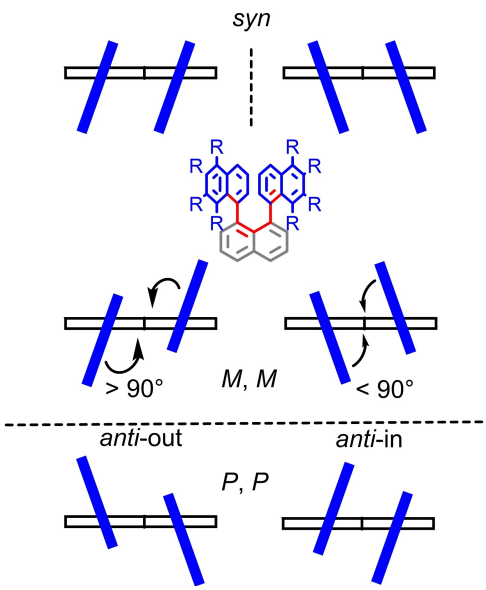

Figure 1. Available conformations for compounds **1,2,6**.

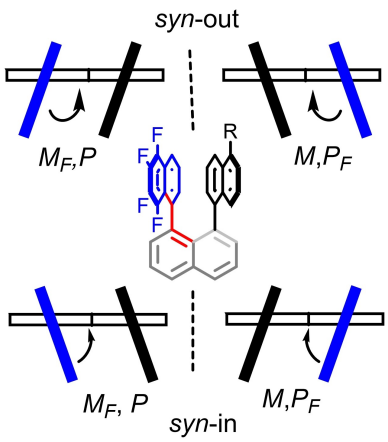

Figure 2. Conformational stereoisomers for the *syn* isomers of compounds **3, 4, 5**. The blue ring represents the 5,6,7,8-tetrafluoro-1-napthyl ring. The corresponding stereochemical descriptor contains the subscript F.

© 2021 The Authors. European Journal of Organic Chemistry published by Wiley-VCH GmbH

conformational cost. This opportunity creates a manifold of available conformations, whose final energy is determined by the best balance between noncovalent attractive/repulsive interactions (Figure 3).

For this reason, the *anti/syn* conformational ratio could provide very good information about the strength and geometries of the electronic interactions. Being the interactions between the two *ipso* rings identical in both isomers, the *syn* isomer should increase when the two *benzo* moieties develop attractive interactions because of the favorable geometrical relationship between the rings.

A variation of the electronic features of the two 1-naphthyl rings and their consequences on the *anti*/*syn* ratio, as well the conformational preference within the *syn* and *anti* isomers, should provide useful information for the interpretation of the factors ruling the noncovalent interactions.

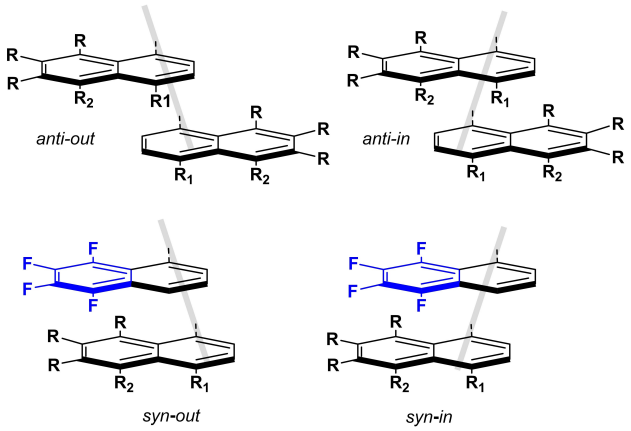

Figure 3. Geometric sketches of the available conformations and stacking geometries in the *anti* and *syn* isomers of compounds **3** (R_1 = Me, R_2 = H), **4** (R_1 = OMe, R_2 = H) and **5** (R_1 = H, R_2 = OMe). The shaded grey lines sketch the 1,8-naphthyl ring.

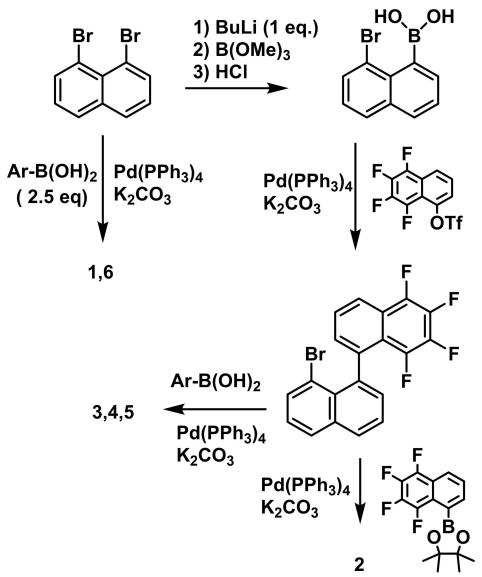

Scheme 2. Synthetic pathways to compounds **1–6**.

Synthesis and kinetic analysis

The synthetic pathways to compounds **1–6** (Scheme 2) involved Suzuki-Miyaura coupling reactions starting from 1,8-dibromo naphthalene with suitable 1-naphthylboronic acids,[24] or a first coupling between 8-bromonaphthyl-1-boronic acid with 5,6,7,8-tetrafluoronaphthalene-1-triflate, followed by reaction with 1-naphthylboronic acids (compounds **3–5**) and with 5,6,7,8-tetrafluoronaphthalene-1-boronpinacolate (compound **2**; full synthetic details are reported in ESI).

All the compounds showed the presence of the *syn* and *anti* isomers in the ambient temperature NMR of the crude, and no sign of line broadening ascribable to chemical exchange was observed up to +120 °C; moreover 1D-EXSY-NMR experiments at the same temperature showed no interconversion, suggesting a diastereomerization barrier higher than 23 kcal/mol. When analyzed with HPLC on achiral reverse-phase columns, all the compounds showed two peaks due to the *anti* and *syn* diastereoisomers. Once separated, the assignment of the *syn* and *anti* isomers of **1**,**2**,**6** was straightforwardly achieved by HPLC analysis on a chiral stationary phase (CSP-HPLC) that allowed resolving the *anti* enantiomeric pair, while the *syn* isomer is a meso form. Both the *syn* and *anti* isomers of compounds **3–5** entail the presence of a pair of enantiomers, so CSP-HPLC cannot be used for their assignment. In these cases, the *syn* and *anti* isomers were identified by means of NMR-NOE experiments (see Figures S3–S5 of ESI for details).

The diastereomerization barriers were determined by standard kinetic analysis using NMR samples of a single isomer in tetrachloroethane-d_2 (TCE-d_2) and DMSO-d_6, by measuring the grow of the second isomer at fixed temperatures as a function of time to determine the kinetic rate constant for diastereomerization, hence the diastereomerization $\Delta G^{\neq}$ (see ESI for details). The samples were then heated to +125 °C for a week to reach the thermodynamic equilibrium (Table 1).

All the diastereomerization barriers exceed the 27 kcal/mol value, so the isomers are conformationally stable at ambient temperature. Because of the higher symmetry, the rotation of a single ring in **1**,**2**,**6** converts the *anti* into the *syn* isomer, so the observed diastereomerization rate constants have to be halved to compare the energy of rotation of a single ring in **1**,**2**,**6** with the observed *syn-anti* barriers of compounds **3–5**. The diastereomerization energy for compound **2** is higher because of the larger steric hindrance of the 8-fluorine with respect to the 8-hydrogen in the transition state. The difference (3.4 kcal/mol) is in good agreement with the steric parameter of fluorine (B value = 4.4).[25] The diastereomerization barriers for compounds **3–5** are due to the rotation of the non-fluorinated ring, which has a lower barrier with respect to the rotation of the tetrafluoro-naphthyl ring (the latter barrier cannot be monitored by NMR in compounds **3**,**4**,**5** because it is an enantiomerization barrier). The experimental values are very similar, but not identical within the experimental error. The difference measured between the 4-metoxylnaphthyl (**4**) and the 5-OMe-naphthyl compounds (**5**) can be attributed to a lower stabilization of the ground state due to the absence of the electron donating properties of the OMe moiety.[13d]

© 2021 The Authors. European Journal of Organic Chemistry published by Wiley-VCH GmbH

Table 1. Summary of *anti*/*syn* ratio for compounds **1–6**, and diastereomerization energies (in kcal/mol).

Compound	*anti*:*syn* TCE +125 °C	*anti*:*syn* DMSO +125 °C	Diast. $\Delta G^{\neq}$ (TCE)[a]
1	76:24	75:25	27.7[b] (+71, +82 °C) 28.2[c] (+71, +82 °C)
2	78:22	66:34	31.3[b] (+113, +118 °C) 31.8[c] (+113, +118 °C)
3	60:40	51:49	29.8 (+92, +102 °C)
4	68:32	58:42	29.7 (+111, +119 °C)
5	54:46	51:49	29.5 (+96, +108 °C)
6	73:27	75:25	28.6[b] (+87 °C) 29.1[c] (+87 °C)

[a] *anti* to *syn* reaction. [b] Measured from kinetic analysis. [c] Derived using k/2 to account for the C_2 symmetry.

DFT calculations

The geometries and relative stability of the various conformations was evaluated by means of DFT calculations.[26] Having in hand the experimental *syn/anti* ratio for compounds **1–6**, we performed a set of calculations to benchmark the performance of several combinations of functionals and basis sets.[27] Among the tested functionals (B3LYP–D3, ωB97X-D, PBE0-D3, B97-D3, and M06-2X), the M06-2X functional has shown to be the most accurate[28] to reproduce the experimental *syn-anti* ratio of compound **2** (See Table S1 of ESI for details).[29] Full geometry optimizations have been run for all compounds with the M06-2X functional[30] and the 6–31+G(d,p) basis set. The solvent polarity was considered by means of the IEFPCM method[31] using chloroform (ε=4.71) to mimic the low polarity solvent TCE (ε=7.09 at +35 °C)[32] and DMSO (ε=46.82). Single point energies were then obtained at the PCM–M06-2X/6-311++G(2d,p) level of theory (see the Experimental section for details), and also with ωB97X–D and the same basis set, but the agreement with the experimental data was less accurate (See Table S3 in ESI).

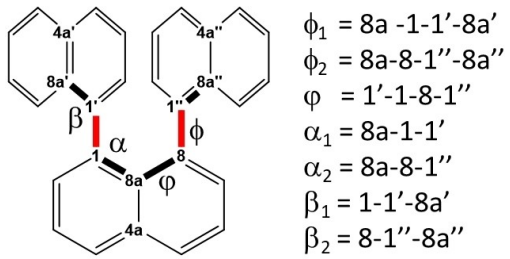

Scheme 3. Definition of the geometrical parameters for conformational analysis.

The key geometrical parameters of the optimized ground state structures (GS) can be derived by the two dihedral angles between the planes of the two naphthalene rings in the 1,8 positions and the central core (ϕ_1 and ϕ_2 in Scheme 3), and to the φ dihedral angle, that is a measurement of the planarity of the 1,8-naphthyl core. Finally, the α and β angles represent a good measurement of the geometrical distortions of the two naphthyl rings (Table 2).

The optimized structures for compound **1**-*anti* (Figure 4) confirmed the existence of two different conformations. The

Table 2. Geometric parameters and relative free energies of the various conformations of compounds **1–6**. Calculations at the PCM–M06-2X/6-311++G(2d,p)//PCM–M06-2X/6-31+G(d,p) in chloroform. Free energies in kcal/mol. See Table S2 in ESI for the geometric parameters with DMSO as the solvent.

Conf.	ϕ_1	ϕ_2	φ	α_1	α_2	β_1	β_2	Inter-ring distance[a]	Calcd. Dipole (D)	G° $CHCl_3$[b]	G° DMSO[b]
1-*anti* (X-ray)	80.1	80.1	-1.8	124.7	124.7	121.1	121.1	3.27	–	–	–
1-*anti*-in	71.2	71.2	5.1	124.8	124.8	121.7	121.7	3.26	0.73	**0.00**	**0.00**
1-*anti*-out	99.4	99.4	19.5	123.2	123.2	122.4	122.4	3.29	0.76	0.21	0.25
1-*syn*	99.2	−83.1	−22.6	122.7	123.4	122.4	118.8	3.30	0.77	1.06	1.15
2-*anti*-in	82.0	82.0	−7.0	124.4	124.4	123.8	123.8	3.26	2.13	**0.00**	**0.00**
2-*syn*	94.7	−86.1	−18.4	123.2	123.7	124.1	121.0	3.21	8.01	0.93	0.70
3-*anti*-in	79.3	77.7	−3.0	125.4	123.6	124.1	121.5	3.29	4.24	**0.00**	**0.00**
3-*syn*-in	80.9	−101.3	−6.7	124.8	124.2	123.8	120.0	3.23	3.76	0.11	0.12
3-*syn*-out	112.8	−72.6	−0.3	125.5	123.7	121.9	121.3	3.29	4.31	1.45	1.48
4-*anti*-in	80.6	80.3	−4.5	125.2	123.6	124.1	121.6	3.26	2.82	**0.00**	**0.00**
4-*syn*-in	80.6	−101.4	−6.7	125.0	124.1	123.8	120.1	3.24	5.04	0.46	0.34
4-*syn*-out	112.7	−72.1	−0.4	125.5	123.7	121.9	121.3	3.31	5.78	1.71	1.77
5-*anti*-in	77.2	−75.8	−1.4	125.3	124.0	124.0	121.0	3.24	5.73	0.16	0.12
5-*syn*-in	82.8	−97.9	−9.1	124.2	124.6	123.7	119.3	3.26	2.19	**0.00**	**0.00**
5-*syn*-out	117.9	−67.6	−5.7	125.1	123.9	122.7	120.7	3.29	2.79	1.59	1.64
6-*anti*-in	67.6	67.4	7.7	124.6	124.6	121.0	121.0	3.21	1.56	**0.00**	**0.00**
6-*syn*	98.1	−83.0	−22.0	122.8	123.5	122.0	118.5	3.20	3.16	0.32	0.61

[a] measured between the planes of the 1-naphthyl rings in the middle of the ring. [b] energies relative to the best conformer within the same compound (in bold).

© 2021 The Authors. European Journal of Organic Chemistry published by Wiley-VCH GmbH

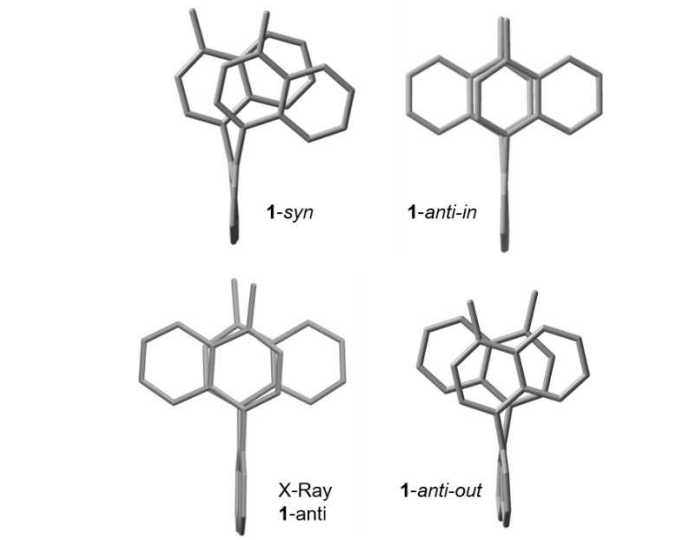

Figure 4. X-ray structure of **1**-*anti*, and DFT-optimized geometries of all conformations [PCM (chloroform) M06-2X/6-311++G(2d,p)//PCM–M06-2X/6-31+G(d,p)].

anti-in conformation has $\phi_1=\phi_2=|71°|$, whereas the *anti-out* has $\phi_1=\phi_2=|99°|$. The **1**-*anti*-in conformation was calculated to be the most stable; instead the **1**-*syn* was calculated to be less stable by 1.06 kcal mol^{-1} and 1.14 kcal mol^{-1} in the low- and high-polarity solvent respectively, in very good agreement with the observed experimental ratio (Table 3).

In the optimized structure for **1**-*anti*-out conformation, the core ring is highly distorted to allow for a larger contact surface between the two naphthyl rings ($\varphi=19°$). Despite the strong distortion of the 1,8-naphthyl ring, this conformation was calculated to be very close in energy to the **1**-*anti*-in. While the **1**-*anti*-in conformation reduces to a minimum the repulsive Coulombic repulsion between the two *benzo* moieties, the **1**-*anti*-out geometry shifts the center of the *ipso* ring over C_{8a} of the second one; in such a way the electron-rich center of benzo moiety juxtapose with the periphery of the other.

The optimized GS structure of the **1**-*syn* isomer shows again a large distortion of the core with $\varphi=22.6°$. This geometry suggests the tendency to modify the geometry of an apparently advantageous parallel-displaced disposition to a situation where other factors lead the achievement of the best energetic compromise. As in the **1**-*anti*-out conformation, the distorted geometry allows the center of the ipso ring to be shifted onto the C8a carbon of the second ring, thus optimizing the interaction between the electron rich part of one naphthalene with an electron-poor counterpart of the second. To consider the possible contributions from dispersive interactions, the corresponding regions were calculated by means of the reduced density gradient approach proposed by Yang.[33] A large portion of the region between the planes of the two 4-methyl-1-naphthyl rings is involved in a weakly attractive interaction in all the three conformations of **1** (Figure 5).[34]

When the extent of the attractive region was considered, the **1**-*syn* isomer should gain stability with respect to the **1**-*anti* because of the larger extent of the contact surface, and for the same reason the **1**-*anti*-out should be more stable than the **1**-*anti*-in. However, this construct is in disagreement with the experimental outcome in solution, being 76:24 the experimental *anti:syn* ratio and the **1**-*anti*-in the preferred conformation in the solid state (Figure 4).[35] The experimental *anti:syn* ratio is thus reasonable to be assigned to electrostatic interactions. In the case of **2**, the 5,6,7,8 fluorine atoms strongly modify the electronic features of the substitution on the *benzo* moiety of the 1-naphthyl ring, that becomes a dyad with electron-rich and electron-poor regions. Only the **2**-*anti*-in conformation was optimized to a ground state ($\alpha=|82°|$) and a noticeable distortion of the core. The **2**-*syn* conformation showed a large distortion of the 1,8-naphthalene too. The interactions between the two rings could be again interpreted by evaluating the dispersive interactions operating between the two rings. Such as **1**, the conclusion obtained for **2** is again in contrast with respect to the experimental *anti:syn* ratio in solution (78:22, see Figure S6 in ESI).

On the other hand, the experimental *anti:syn* ratio of **1** and **2** can be better justified by considering the electrostatic forces to be responsible for the conformational preference, that is driven by the attempt to juxtapose regions with opposite electronic density. In this framework, the **2**-*anti*-in conformation has a clear advantage over the **2**-*syn* (Figure 6), where it is more difficult to get the same arrangement, despite a strong distortion of the naphthyl core. The resulting geometry of the *syn* is therefore the balance of a stabilizing interaction driven by the closeness of opposite polarity regions and the energetically unfavorable distortion of the 1,8-naphthyl core.

Table 3. Summary of experimental and calculated *anti:syn* ratio at +125 °C. Calculations at the M06-2X/6-311++G(2d,p)//M06-2X/6-31+G(d,p), with IEFPCM. Energies in kcal/mol.

Compd.	TCE Exp. *anti:syn*	Exp $\Delta G°$	Calcd[a]. *anti:syn*	DMSO Exp. *anti:syn*	Exp $\Delta G°$	Calcd. *anti:syn*
1	76:24	0.88	83:17	75:25	0.87	82.12
2	78:22	1.00	76:24	66:34	0.52	71:29
3	60:40	0.35	49:51	51:49	0.03	49:51
4	68:32	0.60	60:40	58:42	0.26	57:43
5	54:46	0.13	42:58	51:49	0.03	43:57
6	73:27	0.78	60:40	75:25	0.86	69:31

[a] Calculations run with $CHCl_3$ as a solvent for IEFPCM.

© 2021 The Authors. European Journal of Organic Chemistry published by Wiley-VCH GmbH

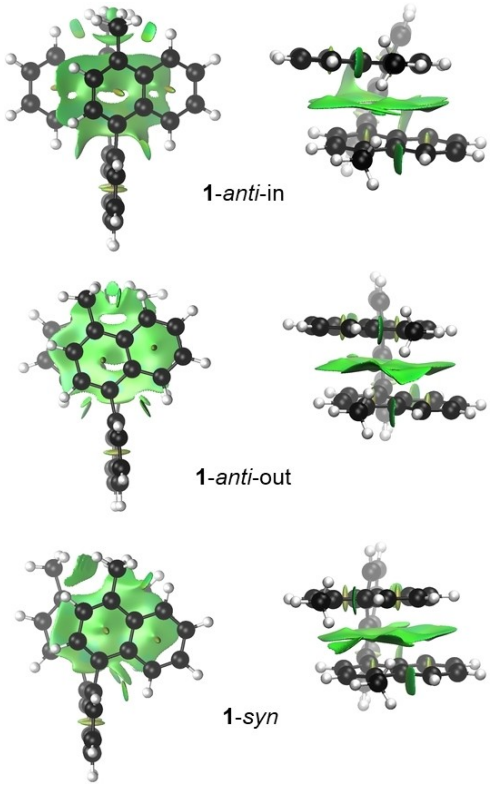

Figure 5. Plot of the noncovalent interactions of compound **1**.

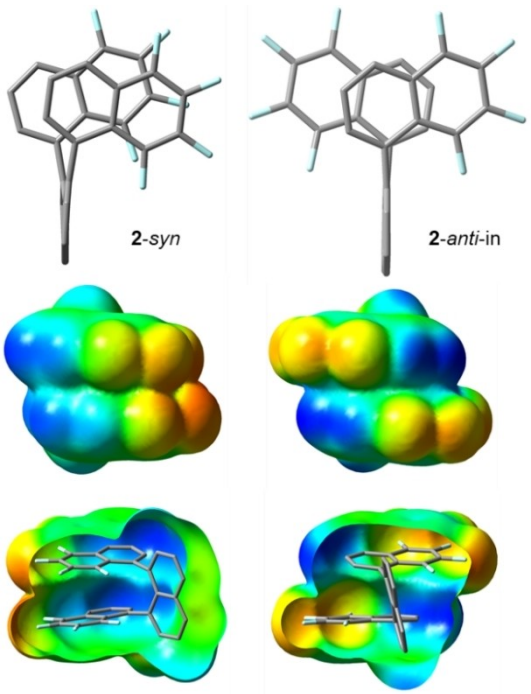

Figure 6. Optimized geometries for compound **2** and electrostatic surfaces (Isovalues at 10^{-4} e^{-}/au^{3}). Hydrogens were removed for clarity.

DFT calculations correctly simulate the experimental ratio, and also the effect of the more polar solvent DMSO that stabilize the *syn* isomer with respect to the *anti* because of the higher dipole moment (Table 3). The **2**-*anti*-out conformation was not optimized to a ground state. In that case the two electron-poor regions (see Figure 6, right) would be driven closer in space by the raise of the α angles above |90°|, with a simultaneous loss of the advantageous electrostatic interactions.

These considerations apply well also to compound **1** (see Figure S9 of ESI), where the distortion of the *syn* isomer (and of the *anti-out*) allow for a better match of regions with opposite electrostatic potential. However, the two naphthyl rings of **1** do not have a very strong unbalance in the electron distribution within each ring. The core distortion does not occur in the **1**-*anti*-in conformation because in this geometry the contact surface is comparable with the *anti*-out conformation, and the center of the *ipso* ring lies above the C_{4a}-C_{8a} bond.

In the last C_2-symmetric compound **6**, the electronic distribution on the benzo moieties is reversed with respect to **2**, because of the 5-methoxy moiety. Nevertheless, the same considerations applied to **1** and **2** can be used for **6** (see Figure S12 of ESI). The *anti*-in conformer is the only GS optimized for the *anti* isomer, and its geometry shows the lowest skew angle (67°). This is the result of the displacement of the two electron-rich rings at the maximum available distance, to relieve the electrostatic repulsion and to better arrange a possible *ipso-benzo* interaction. Also the **6**-*syn* isomer shows high distortion of the core to better arrange the regions of opposite polarity.

When considering the unsymmetrically substituted compounds **3–5**, the 5,6,7,8-tetrafluoro-1-naphthyl ring is a constant, whereas the electronic features, of the second 1-naphthyl ring, are modified by the presence of the 4-methyl, 4-OMe and 5-OMe moieties. The occurrence of the simultaneous presence of the 5,6,7,8-tetrafluoro-1-naphthyl and 4-methynaphthyl rings in compound **3** leads to a more populated *syn* isomer (40% in TCE-d_2 and 49% in DMSO-d_6) with respect to both compounds **1** and **2**. The same occurs for compounds **4** and **5** (Table 3).

As for **2**, only the **3**-*anti*-in conformation was optimized to a GS with a very similar energy to the **3**-*syn*-in conformation; both conformations are much more stable than the **3**-*syn*-out. This trend reproduces the experimental ratio very well (*anti*/*syn* 60:40 in TCE-d_2).

When the electrostatic surfaces are analyzed (Figure 7), it appears again that the driving force is the possibility to correctly arrange regions with the opposite polarity. In the **3**-*syn*-in conformation, the best disposition can be reached without a strong distortion of the core, with a gain in conformational energy that leads to a more populated *syn* isomer. This interpretation can be checked by changing the electronic feature of the 1-naphthyl ring. Compounds **4** and **5** bear a methoxy moiety in position 4 or in position 5 of the 1-naphthyl ring. The strong electron donating group (EDG) raises the electron density on one naphthalene, while keeping constant the electron-poor region on the 5,6,7,8-tetrafluoro-1-naphthyl ring. When the *ipso* ring is made more electron rich (compound **4**), the amount of the *syn* isomer decreases, whereas it increases up to 49% when the EDG raises the electron density in the

© 2021 The Authors. European Journal of Organic Chemistry published by Wiley-VCH GmbH

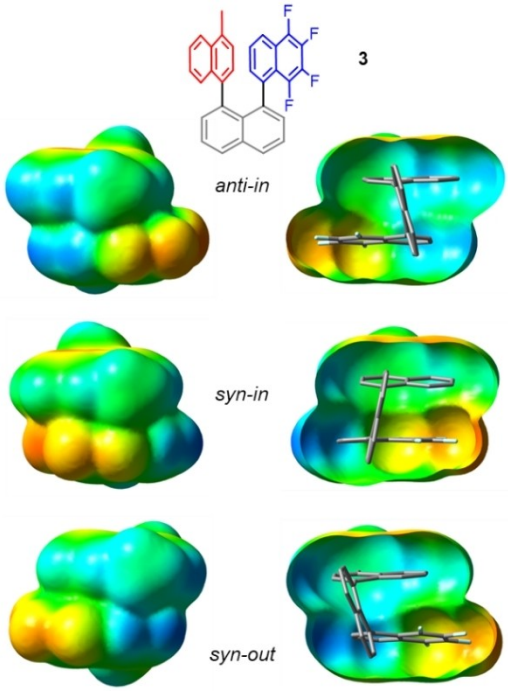

Figure 7. Optimized geometries for compound **3** and electrostatic surfaces (Isovalues at 10^{-4} e^{-}/au^{3}). Hydrogens were removed for clarity.

benzo region (compound **5**). This trend agrees with a stronger electrostatic interaction between the two benzo moieties in **5** with respect to **4**. For the same reason, the **4**-*syn*-in conformation is disfavored with respect to **4**-*anti*-in because of the electrostatic repulsion of the methyl with the border of the ipso ring of the 5,6,7,8-tetrafuoronaphthyl ring (see Figure S10 and Figure S11 of ESI).

The availability of diastereomeric *syn* conformations in compounds **3–5** offers a nice opportunity to evaluate the factors ruling the parallel displaced geometry between the two rings. All the *syn*-out conformations are calculated as much higher in energy with respect to the *syn*-in (Table 2). In both *syn* conformations, the two naphthyl rings are in a parallel displaced arrangement, with very similar inter-ring distances ($\approx$3.3 Å).

However, in the case of the *syn*-in conformation, the center of the 5,6,7,8-tetrafluoronaphthyl moiety is driven above the carbon in position 8a of the other ring (left in Figure 3), while in the *syn*-out conformation the situation is reversed: the center of the electron-rich ring lies above C8a of the 5,6,7,8-tetrafluoro-1-naphthyl ring (Figure 3, right). Within the electrostatic theory, an advantageous interaction is realized when the quadrupole moment of the electron-poor ring (reversed in sign with respect to a standard benzene) interacts with an electron-rich region. This can be realized only in the *syn*-in conformation geometry. Being the steric and dispersive interactions very similar within the two *syn* conformations, the stabilization of the *syn*-in geometry can be evaluated as $\approx$1.5 kcal/mol (i.e. the *syn*-in:*syn*-out energy difference from Table 2). An experimental proof of the preferred conformation of the *syn* isomers can be inferred by the simulation of the ECD spectra, see below).

Conformational analysis of the *syn* isomers

Once resolved on CSP-HPLC, the absolute configuration of the atropisomers was determined by means of the TD-DFT simulation of the ECD spectra (see ESI for full details). Being quite rigid, the ECD spectra of the *anti* isomers (*M*, *M* atropisomer Figure 8, top) showed a strong exciton coupling in the 230–205 nm region ($^{1}B_{b}$ band of naphthalene) due to the same spatial relationship of each naphthyl ring with the naphthalene scaffold.

On the contrary, the ECD spectra of the *syn* isomers (Figure 8, bottom) do not clearly show any exciton coupling because of the opposite sign of the two α angles. This causes the two exciton couplings due to the two different rings to partially compensate because of the opposite sign of the dihedral angles with the 1,8-naphthyl ring,[36] and only the residual difference is present in the experimental spectrum. The weakness of the spectra for the *syn* isomers with respect to the *anti*, and the occurrence of the maximum value of the CD signal of the *syn* isomers in correspondence with the null point of the exciton coupling of the *anti* isomers confirm this hypothesis (see Figure S13 of ESI for a comparison of ECD spectra with the corresponding UV). The UV maxima of absorbance agree with the sum of naphthalene spectra, so any charge-transfer

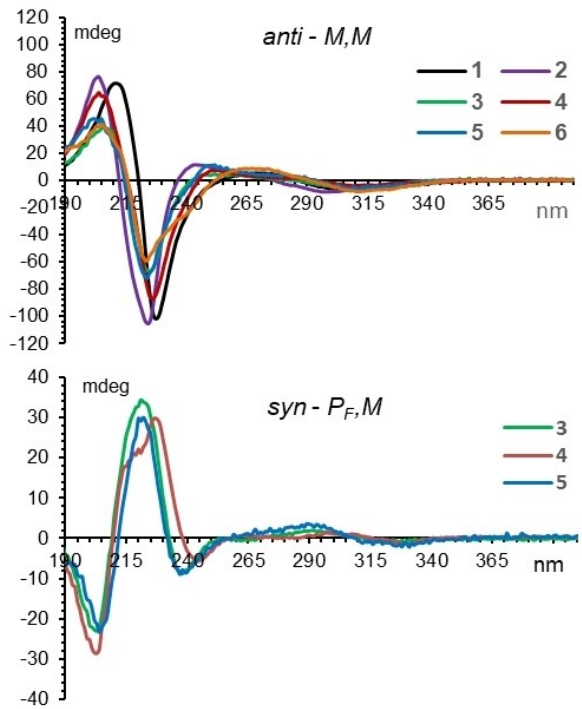

Figure 8. ECD spectra of the (*M*, *M*) – *anti* (top) and (P_F,*M*)-*syn* (bottom) isomers of compounds **1–6** (only compounds **3–5** have optically active syn isomers).

© 2021 The Authors. European Journal of Organic Chemistry published by Wiley-VCH GmbH

interaction between the two facing naphthalenes is not evident.

TD-DFT simulations of the ECD spectra allowed for a deeper experimental analysis of the preferred conformations of the *anti* and *syn* isomers. The two ancillary rings are not perpendicular to the naphthyl core, and the shape and intensity of the ECD spectrum changes as a function of the ϕ_1 and ϕ_2 dihedral angles,[37] within the two available combinations for the *anti* and *syn* isomers.

When the *anti* isomers are considered, only compound **1** has two minima energies, while the *anti*-in conformation was calculated to be the only ground state for compounds **2–6**. TD-DFT calculations of the **1**-*anti*-in and **1**-*anti*-out conformations showed slightly different shape due to the change of the dihedral angles with the 1,8-naphthyl scaffold. The experimental spectrum was correctly simulated using the 59:41 ratio suggested by calculations (see ESI), but a better simulation was obtained when a 90:10 ratio (*anti*-in:*anti*-out) was used (see Figure S14 of ESI). This result suggests that the population of **1**-*anti*-out was overestimated by calculations, and the **1**-*anti*-in is indeed the most populated conformation in solution. In the cases of the **2–6** *anti* isomers, all the ECD simulations of the *anti*-in conformers agree very well with the experimental spectrum (see Figures S15, S16, S17, S19, S21 of ESI). It should be noted that the amplitude of the exciton coupling of **6**-*anti* is smaller with respect to **1**-*anti* and **2**-*anti;* this is in good agreement with the smaller skew angles suggested by calculations.

A different situation was encountered in the simulation of the ECD spectra of the *syn* atropisomers of **3–5**. The spectra calculated for the *syn*-in and *syn*-out conformations of **3** are almost mirror images (Figure 9). This is due to the different strength of the two exciton couplings within the two "isolated" binaphthyl systems, i.e. the 5,6,7,8-tetrafuoronaphthyl/1-naphthyl branch, and the 4-methylnaphthyl/8-naphthyl one. In each separate dipole combination, the exciton coupling, due to a dihedral angle smaller than $|90°|$ prevails over the second exciton coupling, whose angle is larger than $|90°|$.[38] The experimental ECD spectrum and the theoretical ratio employed in the TD-DFT simulation are therefore very good sensors of the preferred conformation of the *syn* isomers. An example of such a simulation is reported in Figure 9 for compound **3**-*syn* (P_F, *M* atropisomer, see Figures S18, S19 and S22 of ESI for compounds **4**-*syn* and **5**-*syn*).

An excellent simulation was obtained only when considering a conformational ratio strongly biased towards the *syn*-in conformation, as suggested by the calculated energies of Table 2. This occurrence is an experimental proof of the higher stability of the *syn*-in conformation. A very similar situation was observed for compounds **4**-*syn* and **5**-*syn*.

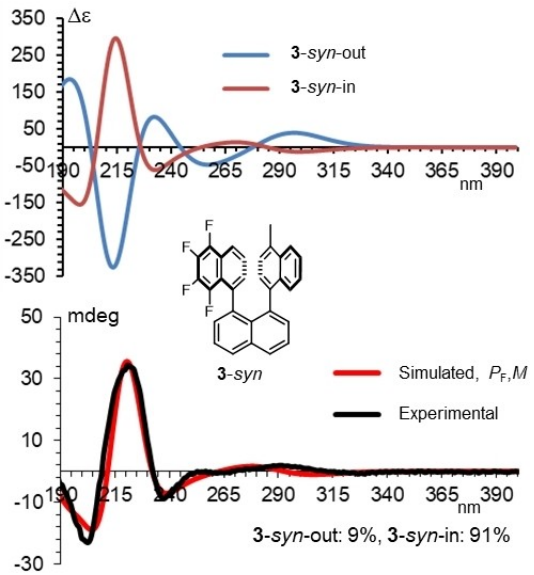

Figure 9. Top: TD-DFT simulations for the two conformations of **3**-*syn* (TD-CAM–B3LYP/6-311++G(2d,p)//M06-2X/6-31+G(d,p)) are shown. Bottom: comparison with the experimental spectrum and percentages used for the simulation.

Conclusion

By using a combination of DFT calculation, NMR and ECD spectra we have performed a detailed conformational analysis that allowed a rationalization of the noncovalent interactions between two naphthyl rings kept in a face-to-face relationship with the 1,8-naphthyl scaffold. The experimental *syn/anti* ratio can be well rationalized by the optimization of electrostatic interactions between the two rings, whereas dispersive interactions seem to play a minor contribution. When the *syn* isomers yielded two diastereomeric optically active conformations, the simulation of the ECD spectra allowed to determine that the best staking geometry is again driven by the optimization of the electrostatic interactions.

Experimental Section

Chemicals were purchased by Sigma Aldrich and Alfa Aesar and used without further purification. 5,6,7,8-Tetrafluoronaphthalen-1-ol[39] and 1,8-dibromonaphthalene[40] were prepared according to known procedures. Diethyl ether and THF have been dried by distillation on Na/benzophenone. Chromatography employed the following stationary phases: Silica gel 60 F254 for the TLC and silica gel 60 Å (230–400 mesh) for pre-purification. All the reactions were performed in dried glassware and under dry nitrogen atmosphere. Glassware was dried at +70 °C for at least 3 hours immediately before use. Semi-preparative HPLC purification was achieved using a Waters 600 pump with a Waters 2487 UV detector. Detection wavelength was 254 nm. A Phenomenex Luna C8 (5 μm, 100 Å, 250×10.0 mm) semi-preparative HPLC column or Phenomenex Polar-RP (4 μm, 80 Å, 250x21.2 mm) were used to purify the compounds using mixtures of CH_3CN and H_2O as eluents. Resolution of the enantiomeric pairs were obtained on cellulose-based chiral stationary phases (Chiralcel OD–H, Chiralcel OG, Phenomenex LUX Cellulose-2) and mixture of hexane/isopropanol as eluents (see ESI for full synthetic and separation details, and for spectroscopic characterization)

NMR spectra were recorded using a spectrometer operating at 14.4 T (600 MHz for ^1H, 150.8 for ^{13}C and 564.2 MHz for ^{19}F). Chemical shifts are given in ppm relative to the internal standard TMS (^1H

© 2021 The Authors. European Journal of Organic Chemistry published by Wiley-VCH GmbH

and ^{13}C), and to the external standard $CFCl_3$ (^{19}F). The ^{13}C NMR spectra were acquired under proton decoupling conditions with a 36000 Hz spectral width, 5.5 μs (60° tip angle) pulse width, 1 s acquisition time and 5 s delay time. A line broadening function of 1–2 Hz was applied before the Fourier transformation. ^{13}C spectra of compounds **2–5** were also obtained with ^{19}F broadband decoupling, in order to determine the chemical shifts of the fluorinated carbons. The assignment of the ^{13}C signals was obtained by means of DEPT sequences. Assignments of the *syn* and *anti* isomers of compounds **3–5** were achieved by NOE spectra, recorded at 600 MHz using the DPFGSE sequence[41] and a 50 Hz selective pulse with an R-SNOB shape[42] (See ESI for full details of the assignment). Kinetic analysis of the *anti/syn* diastereomerization barriers were obtained by keeping the NMR sample at high temperature, and recording the ^1H spectra at fixed periods of time. A first-order kinetic equation at equilibrium yielded the rate constants, that were used to derive the $\Delta G^{\neq}$ by means of the Eyring equation. Temperature calibrations within the NMR probe were performed before the experiments, using a digital thermometer and a Cu/Ni thermocouple inserted into a dummy sample filled with TCE. The conditions were kept as identical as possible with the subsequent work, in particular the sample was not spun and the gas flow was the same as that used during the temperature calibration. The uncertainty in temperature measurements can be estimated as ± 1 °C. When an external oil bath was used to heat the NMR sample, the same thermocouple was used to monitor the temperature.

ECD spectra were recorded at $+25$ °C in far-UV HPLC-grade acetonitrile solutions. The concentrations of the samples (about 10^{-4} M) were tuned by dilution of a mother solution ($1{\cdot}10^{-3}$ M) to obtain a maximum absorbance of about $0.8 \div 0.9$ in the UV spectrum using a 0.2 cm path length. The spectra were recorded in the 190–400 nm interval as the sum of 16 spectra. The spectra shown in Figure 8 were normalized in intensity using the intensities of the UV spectra, in which the maximum absorbance in the 215–225 nm range was normalized to A = 1.0.

Ground state optimizations and transition states were obtained by DFT computations performed by the Gaussian 16 rev. A.03 software suite[26] using standard parameters. Full optimization and frequency analysis for ground states and transition states employed the M06-2X functional[30] and the 6–31 + G(d,p) basis set. The IEFPCM approach was used to account for the solvent contribution. The analysis of the vibrational frequencies showed the absence of imaginary frequencies for the ground states, and the presence of one imaginary frequency for each transition state. Visual inspection of the corresponding normal mode validated the identification of the transition states. The frequencies were scaled by 0.967[43] and the RRHO approximation[44] was used to moderate the effect of the low-energy vibrators on the evaluation of the entropic correction.[45] Single point energies were calculated at the M06-2X/6-311 + + g(2d,p) level and ωB97X–D/6-311 + + g(2d,p).[46] The ZPE and thermal corrections obtained with M06-2X at the lower level were used to derive the Gibbs free energies reported in Table 2 and in Table S3 of the ESI. The ECD spectra of the optically active isomers were calculated using the TD-DFT approach.[47] The electrostatic surfaces were calculated and shown using Gauss View.[48] For all the representations, the same range was used for the color code (from $-3.7e^{-2}$ to $3.7e^{-2}$; red and blue, respectively). The theoretical ECD spectra of the GS conformations were obtained with four different functionals (CAM–B3LYP,[49] ωB97X–D,[46] BH&HLYP[50] and M06-2X[30]) with the same 6–311 + + G(2d,p) basis set, in order to have data redundancy, and to enhance reliability.[51] For each conformation 70 discrete transitions were calculated, and the ECD spectrum was obtained by convolution of Gaussian shaped lines (0.5 eV half-height line width).[48]

The simulated spectra resulting from the Boltzmann averaged sum of the conformations (relative energies from Table 2) were red-shifted by 6–12 nm to get the best simulations with the experimental spectra. All the simulations are reported in Figures S15–S23 of ESI.

Deposition Number 2055991 (for **1**-*anti*) contains the supplementary crystallographic data for this paper. These data are provided free of charge by the joint Cambridge Crystallographic Data Centre and Fachinformationszentrum Karlsruhe Access Structures service www.ccdc.cam.ac.uk/structures.

Acknowledgements

The University of Bologna is gratefully acknowledged for financial support (RFO funds 2018 and 2019).

Conflict of Interest

The authors declare no conflict of interest.

Keywords: DFT calculations · Electronic circular dichroism · NMR spectroscopy · Noncovalent interactions

[1] F. Cozzi, M. Cinquini, R. Annunziata, T. Dwyer, J. S. Siegel, *J. Am. Chem. Soc.* **1992**, *114*, 5729–5733.
[2] a) E. A. Meyer, R. K. Castellano, F. Diederich, *Angew. Chem. Int. Ed.* **2003**, *42*, 1210–1250; *Angew. Chem.* **2003**, *115*, 1244–1287; b) S. L. Cockroft, J. Perkins, C. Zonta, H. Adams, S. E. Spey, C. M. R. Low, J. G. Vinter, K. R. Lawson, C. J. Urch, C. A. Hunter, *Org. Biomol. Chem.* **2007**, *5*, 1062–1080.
[3] D. B. Amabilino, J. F. Stoddart, *Chem. Rev.* **1995**, *95*, 2725–2829.
[4] G. B. Jones, *Tetrahedron* **2001**, *57*, 7999–8016.
[5] a) M. Weck, A. R. Dunn, K. Matsumoto, G. W. Coates, E. B. Lobkowsky, R. H. Grubbs, *Angew. Chem. Int. Ed.* **1999**, *38*, 2741–2745; *Angew. Chem.* **1999**, *111*, 2090–2911; b) G. J. Gabriel, S. Sorey, B. L. Iverson, *J. Am. Chem. Soc.* **2005**, *127*, 2637–2640; c) K. Reichenbächer, H. I. Süss, J. Hulliger, *Chem. Soc. Rev.* **2005**, *34*, 22–30; d) J. D. Dunitz, A. Gavezzotti, *Angew. Chem. Int. Ed.* **2005**, *44*, 1766–1787; *Angew. Chem.* **2005**, *117*, 1796–1819.
[6] R. Thakuria, N. K. Nath, B. K. Saha, *Cryst. Growth Des.* **2019**, *19*, 523–528.
[7] M. L. Waters, *Curr. Opin. Chem. Biol.* **2002**, *6*, 736–741.
[8] P. A. Williams, J. Cosme, A. Ward, H. C. Angove, D. M. Vinkovic, H. Jhoti, *Nature* **2003**, *424*, 464–468.
[9] a) J. Houser, S. Kozmon, D. Mishra, Z. Hammerová, M. Wimmerová, J. Koča, *Chem. Eur. J.* **2020**, 26, 10769–10780; b) K. L. Hudson, G. J. Bartlett, R. C. Diehl, J. Agirre, T. Gallagher, L. L. Kiessling, D. N. Woolfson, *J. Am. Chem. Soc.* **2015**, *137*, 15152–15160; c) S. Vandenbussche, D. Diaz, M. C. Fernandez-Alonso, W. Pan, S. P. Vincent, G. Cuevas, F. J. Cañada, J. Jimenez Barbero, K. Bartik, *Chem. Eur. J.* **2008**, *14*, 7570–7578; d) Z. R. Laughrey, S. E. Kiehna, A. J. Riemen, M. L. Waters, *J. Am. Chem. Soc.* **2008**, *130*, 14625–14633.
[10] a) W. R. Zhuang, Y. Wang, P. F. Cui, L. Xing, J. Lee, D. Kim, H. L. Jiang, Y. K. Oh, *J Control Release* **2019**, 294–311–326; b) G. Kryger, I. Silman, J. L. Sussman, *J. Physiol.* **1998**, *92*, 191–194.
[11] a) C. A. Hunter, K. R. Lawson, J. Perkins, C. J. Urch, *J. Chem. Soc. Perkin Trans. 2* **2001**, 651–669; b) M. O. Sinnokrot, C. D. Sherrill, *J. Phys. Chem. A* **2006**, *110*, 10656–10668; c) S. E. Wheeler, *J. Am. Chem. Soc.* **2011**, *133*, 10262–10274.
[12] a) C. A. Hunter, J. K. M. Sanders, *J. Am. Chem. Soc.* **1990**, *112*, 5525–5534; b) S. L. Cockroft, C. A. Hunter, K. R. Lawson, J. Perkins, C. J. Urch, *J. Am. Chem. Soc.* **2005**, *127*, 8594–8595; c) S. L. Cockroft, C. A. Hunter, *Chem. Soc. Rev.* **2007**, *36*, 172–188.
[13] a) F. Cozzi, M. Cinquini, R. Annunziata, J. S. Siegel, *J. Am. Chem. Soc.* **1993**, *115*, 5330–5331; b) F. Cozzi, F. Ponzini, R. Annunziata, M. Cinquini,

© 2021 The Authors. European Journal of Organic Chemistry published by Wiley-VCH GmbH

J. S. Siegel, *Angew. Chem. Int. Ed.* **1995**, *34*, 1019–1020; *Angew. Chem.* **1995**, 107, 1092–1094; c) F. Cozzi, R. Annunziata, M. Benaglia, M. Cinquini, L. Raimondi, K. K. Baldridge, J. S. Siegel, *Org. Biomol. Chem.* **2003**, *1*, 157–162; d) F. Cozzi, R. Annunziata, M. Benaglia, K. K. Baldridge, G. Aguirre, J. Estrada, Y. Sritana-Anant, J. S. Siegel, *Phys. Chem. Chem. Phys.* **2008**, *10*, 2686–2694.
[14] M. O. Sinnokrot, C. D. Sherrill, *Phys. Chem. A* **2003**, *107*, 8377–8379.
[15] S. E. Wheeler, K. N. Houk, *J. Am. Chem. Soc.* **2008**, *130*, 10854–10855.
[16] S. E. Wheeler, *Acc. Chem. Res.* **2013**, *46*, 1029–1038.
[17] S. Grimme, *Angew. Chem. Int. Ed.* **2008**, *47*, 3430–3434. *Angew. Chem.* **2008**, *120*, 3478–3483.
[18] C. R. Martinez, B. L. Iverson, *Chem. Sci.* **2012**, *3*, 2191–2201.
[19] a) R. L. Clough, J. D. Roberts, *J. Am. Chem. Soc.* **1976**, *98*, 1018–1020; b) L. Lunazzi, M. Mancinelli, A. Mazzanti, *J. Org. Chem.* **2007**, *72*, 5391–5394.
[20] L. Lunazzi, M. Mancinelli, A. Mazzanti, *J. Org. Chem.* **2007**, *72*, 10045–10050.
[21] In this case the M/P terminology cannot be used to assign the two enantiomers. The *+sc* and *+sc* stereochemical descriptors should be used instead. See B. Testa, *Principles of organic stereochemistry. In: Studies in Organic Chemistry* Volume 6, (Eds. P. G. Gassman) Marcel Dekker inc, New York, **1979**, Chapter 9.
[22] a) S. Paliwal, S. Geib, C. S. Wilcox, *J. Am. Chem. Soc.* **1994**, *116*, 4497–4498; b) W. R. Carroll, P. Pellechia, K. D. Shimizu, *Org. Lett.* **2008**, *10*, 3547–3550; c) W. B. Motherwell, J. Moïse, A. E. Aliev, M. Nič, S. J. Coles, P. N. Horton, M. B. Hursthouse, G. Chessari, C. A. Hunter, J. G. Vinter, *Angew. Chem. Int. Ed.* **2007**, *46*, 7823–7826, *Angew. Chem.* **2007**, 119, 7969–7972.
[23] J. W. G. Bloom, S. E. Wheeler, *Angew. Chem. Int. Ed.* **2011**, *50*, 7847–7849; *Angew. Chem.* **2011**, *123*, 7993–7995.
[24] G. Pieters, V. Terrasson, A. Gaucher, D. Prim, J. Marrot, *Eur. J. Org. Chem.* **2010**, 5800–5906.
[25] A. Mazzanti, L. Lunazzi, R. Ruzziconi, S. Spizzichino, M. Schlosser, *Chem. Eur. J.* **2010**, *16*, 9186–9192.
[26] Gaussian 16, Revision A.03, M. J. Frisch, G. W. Trucks, H. B. Schlegel, G. E. Scuseria, M. A. Robb, J. R. Cheeseman, G. Scalmani, V. Barone, G. A. Petersson, H. Nakatsuji, X. Li, M. Caricato, A. V. Marenich, J. Bloino, B. G. Janesko, R. Gomperts, B. Mennucci, H. P. Hratchian, J. V. Ortiz, A. F. Izmaylov, J. L. Sonnenberg, D. Williams-Young, F. Ding, F. Lipparini, F. Egidi, J. Goings, B. Peng, A. Petrone, T. Henderson, D. Ranasinghe, V. G. Zakrzewski, J. Gao, N. Rega, G. Zheng, W. Liang, M. Hada, M. Ehara, K. Toyota, R. Fukuda, J. Hasegawa, M. Ishida, T. Nakajima, Y. Honda, O. Kitao, H. Nakai, T. Vreven, K. Throssell, J. A. Montgomery, Jr., J. E. Peralta, F. Ogliaro, M. J. Bearpark, J. J. Heyd, E. N. Brothers, K. N. Kudin, V. N. Staroverov, T. A. Keith, R. Kobayashi, J. Normand, K. Raghavachari, A. P. Rendell, J. C. Burant, S. S. Iyengar, J. Tomasi, M. Cossi, J. M. Millam, M. Klene, C. Adamo, R. Cammi, J. W. Ochterski, R. L. Martin, K. Morokuma, O. Farkas, J. B. Foresman, D. J. Fox, Gaussian, Inc., Wallingford CT, 2016.
[27] J Řezáč, P Hobza *Chem. Rev.* **2016**, *116*, 5038–5071.
[28] E. G. Hohenstein, S. T. Chill, C. D. Sherrill, *J. Chem. Theory Comput.* **2008**, *4*, 1996–2000.
[29] Also when using a triple-zeta basis set with D3 correction (PBE0-D3/def2-TZVPP), the agreement with the experimental data was less accurate than M06-2X/6-31 + G(d p). W. Wang, Y. Zhang, Y–B. Wang, *Int. J. Quantum Chem.* **2016**, 1–8.
[30] a) Y. Zhao, D. G. Truhlar, *Acc. Chem. Res.* **2008**, *41*, 157–167; b) R. G. Huber, M. A. Margreiter, J. E. Fuchs, S. von Grafenstein, C. S. Tautermann, K. R. Liedl, T. Fox, *J. Chem. Inf. Model.* **2014**, *54*, 1371–1379.
[31] J. Tomasi, B. Mennucci, R. Cammi, *Chem. Rev.* **2005**, *105*, 2999–3093.
[32] N. V. Sastry, A. George, N. J. Jain, P. Bahadur, *J. Chem. Eng. Data* **1999**, *44*, 456–464.
[33] a) E. R. Johnson, S. Keinan, P. Mori-Sanches, J. Contreras-Garcia, A. J. Cohen, W. Yang, *J. Am. Chem. Soc.* **2010**, *132*, 6498–6506; b) J. Contreras-Garcia, E. R. Johnson, S. Keinan, R. Chaudret, J.-P. Piquemal, D. N. Beratan, W. Yang, *J. Chem. Theory Comput.* **2011**, *7*, 625–632; c) R. A. Boto, F. Peccati, R. Laplaza, C. Quan, A. Carbone, J.-P. Piquemal, Y. Maday, J. Contreras-Garcia, NCIPLOT4: A new step towards a fast quantification of noncovalent interactions, https://github.com/juliacontrerasgarcia/nciplot.
[34] VMD software rel. 1.9.3. W. Humphrey, A. Dalke, K. Schulten, K. VMD: Visual Molecular Dynamics, *J. Mol. Graphics* **1996**, *14*, 33 − 38. The color code is related to the −0.05 to 0.05 range of sign(λ2)ρ.
[35] Although the crystal packing could alter the preferred geometry, the most populated conformation in solution is usually that present in the solid state. For an example see: C. Coluccini, S. Grilli, L. Lunazzi, A. Mazzanti *J. Org. Chem.* **2003**, *68*, 7266–7273.
[36] For a similar case see: L. Bernardi, G. Bolzoni, M. Fochi, M. Mancinelli, A. Mazzanti *Eur. J. Org. Chem.* **2016**, 3208–3216.
[37] a) G. Pescitelli, L. Di Bari, N. Berova, *Chem. Soc. Rev.* **2011**, *40*, 4603–4625; b) L. Di Bari, G. Pescitelli, P. Salvadori, *J. Am. Chem. Soc.* **1999**, *121*, 7998–8004.
[38] S. F. Mason, R. H. Seal, D. R. Roberts, *Tetrahedron* **1974**, *30*, 1671.
[39] G. W. Gribble, C. S. Le Houllier, M. P. Sibi, R. W. Allen *J. Org. Chem.* **1985**, *50*, 1611–1616.
[40] D. Seyferth, S. C. Vick, *J. Organomet. Chem.* **1977**, *141*, 173–187.
[41] J. Stonehouse, P. Adell, J. Keeler, A. J. Shaka, *J. Am. Chem. Soc.* **1994**, *116*, 6037–6038.
[42] E. Kupče, J. Boyd, I. D. Campbell, *J. Magn. Reson. Ser. B* **1995**, *106*, 300.
[43] I. M. Alecu, J. Zheng, Y. Zhao, D. G. Truhlar, *J. Chem. Theory Comput.* **2010**, *6*, 2872–2887.
[44] S. Grimme, *Chem. Eur. J.* **2012**, *18*, 9955–9964.
[45] A cutoff value of 100 cm^{-1} was used within the Goodvibes software. G. Luchini, J. V. Alegre-Requena, Y. Guan, I. Funes-Ardoiz, R. S. Paton, GoodVibes: GoodVibes 3.0.1 http://doi.org/10.5281/zenodo.595246, **2019**.
[46] J.-D. Chai, M. Head-Gordon, *Phys. Chem. Chem. Phys.* **2008**, *10*, 6615–6620.
[47] a) S. Superchi, P. Scafato, M. Górecki, G. Pescitelli, *Curr. Med. Chem.* **2018**, *25*, 287; b) M. Srebro-Hooper, J. Autschbach, *Annu. Rev. Phys. Chem.* **2017**, *68*, 399; c) G. Pescitelli, T. Bruhn, *Chirality* **2016**, *28*, 466–474; d) C. Adamo, D. Jacquemin, *Chem. Soc. Rev.* **2013**, *42*, 845–856; e) D. Casarini, A. Mazzanti, *WIREs Comput. Mol. Sci.* **2012**, *2*, 613–641.
[48] Gausswiew 6.0.16, Semichem, Inc. 2000–2016.
[49] T. Yanai, D. Tew, N. Handy, *Chem. Phys. Lett.* **2004**, *393*, 51–57.
[50] In Gaussian 16 the BH&HLYP functional has the form: $0.5*^{EXHF} + 0.5*^{EXLSDA} + 0.5*\Delta EX^{Becke88} + EC^{LYP}$.
[51] M. Mancinelli, R. Franzini, A. Renzetti, E. Marotta, C. Villani, A. Mazzanti, *RSC Adv.* **2019**, *9*, 18165–18175.

Manuscript received: January 14, 2021
Revised manuscript received: March 9, 2021
Accepted manuscript online: March 18, 2021

© 2021 The Authors. European Journal of Organic Chemistry published by Wiley-VCH GmbH